Experimental and theoretical study of excitonic transition energies in GaAs/$Al_xGa_{1-x}As$ quantum wells

G. Oelgart
BOS-GmbH Berlin, Ostendstrasse 1-14, D-12459 Berlin, Federal Republic of Germany

M. Proctor, D. Martin, F. Morier-Genaud, and F.-K. Reinhart
Institut de Micro- et Optoélectronique, Ecole Polytechnique Fédérale de Lausanne, PHB-Ecublens, CH 1015 Lausanne, Switzerland

B. Orschel
Fachbereich Physik der Universität Leipzig, Linnéstrasse, 5, D-04103 Leipzig, Federal Republic of Germany

L. C. Andreani
Dipartimento di Fisica "Alessandro Volta", Università di Pavia, via Bassi 6, I-27100 Pavia, Italy

H. Rhan*
Sektion Physik, Universität München, Geschwister-Scholl-Platz 1, D-80539 München, Federal Republic of Germany
(Received 1 June 1993; revised manuscript received 18 October 1993)

High-quality molecular-beam-epitaxy-grown decoupled GaAs-(Al,Ga)As multiple quantum wells (MQW) of various well thickness ($2.7 \leq L_W \leq 11.9$ nm; $x \approx 0.3$) and different barrier compositions ($0.12 \leq x \leq 1$; $L_W \approx 11$ nm) have been studied by x-ray diffraction (XRD), photoluminescence excitation, and emission (PL). The temperature dependence of the MQW properties has also been studied. The well width and barrier composition of the MQW were obtained by XRD and PL, respectively. 2*s*-excitonic features and the free electron-hole sublevel transitions can be resolved. We compare the 1*s*-2*s* energy difference and the ground-state binding energies of the heavy- and light-hole excitons with a recent accurate theory of exciton binding energies, taking the structure parameters from an independent determination. Experimental and theoretical values of the heavy- and light-hole exciton binding energies are found to agree within 1 meV. The theoretically predicted and experimentally observed excitonic transition energies associated with the lowest ($n = 1$) electron, heavy-hole, and light-hole sublevels agree well, if the theoretical approach includes the split-off valence band. Interpolation formulas for the heavy- and light-hole ground-state exciton binding energies and for the $n = 1$ electron, heavy-, and light-hole sublevel energies are given.

I. INTRODUCTION

Although progress has been made in predicting the exciton binding and the sublevel energies in multiple quantum-well structures (MQW's) there is still considerable uncertainty concerning the theoretical approach and the parameter sets used.[1-5] Two steps are required in order to calculate the optical transition energies of the excitons. The first is a calculation of the sublevel energies at $k = 0$. This can be done in an envelope-function approach (cf. the Appendix), taking into account the different band parameters in well and barrier materials, nonparabolicity of the bulk conduction band of both constituent materials, and for light-hole levels, coupling to the split-off band.[3,5] Valence-band mixing does not change the position of the sublevels at $k = 0$ in [001]-grown MQW's.

The second step is a calculation of the exciton binding energy, which must be subtracted from the sublevel energy in order to obtain the exciton transition energy. Recently, an accurate theory of excitons in GaAs/(Al,Ga)As quantum wells has been developed.[6,7] This theory simultaneously includes valence-band mixing, Coulomb coupling between excitons belonging to different valence subbands, the nonparabolicity of the bulk conduction band, and the difference in the dielectric constants between well and barrier materials. The approximation of neglecting Coulomb coupling between excitons belonging to different conduction subbands was checked by a separate calculation[8] that neglects the valence-band mixing but includes the coupling between all pairs of conduction and valence subbands. The conduction subband coupling changes the exciton binding energies by less than 0.2 meV in the range of well width considered here (Coulomb coupling between excitons belonging to different valence subbands has a much larger effect, because it is enhanced by valence-band mixing). Also, coupling between light-hole and split-off bands was not included in the exciton binding-energy calculation, although it is important for the light-hole energy levels. The reason is that the exciton binding energy depends on the reduced effective mass that is dominated by the small electron mass (the in-plane light-hole effective mass $\approx 0.21 m_0$ is much larger than the electron effective mass

due to the mass-reversal effect).

The most sensitive part for a determination of the transition energy is the sublevel energies, which may vary depending on the material parameters, the precise value of the total band-gap difference, and the offset ratio. It is the aim of this paper to compare the experimentally and the theoretically determined exciton binding and transition energies in a wide well width range ($2.7 \leq L_W \leq 8.8$ nm; $x \approx 0.3$) and for different barrier heights ($0.12 \leq x \leq 1$; $L_W \approx 11$ nm). Utilizing the independently obtained parameters of the MQW structure, the theoretical predictions are compared with the experimental findings.

II. EXPERIMENTAL DETAILS

The GaAs/(Al,Ga)As MQW were grown by conventional molecular-beam epitaxy techniques at 870 or 970 K. Each sample consists of a 500-nm-thick GaAs buffer layer grown on a [001] oriented Si-doped GaAs substrate, followed by about 50 periods of the MQW, and finally a 100-nm top layer of the barrier alloy. The AlAs content of the $Al_xGa_{1-x}As$ barriers x was determined from the bound exciton peak energy.[9] The period length was directly probed by x-ray diffraction (XRD) and the width of wells (L_W) and barriers (L_B) were obtained by a dynamical simulation procedure. In all samples L_B was chosen so as to ensure that the quantum wells (QW) were effectively decoupled electronically. To avoid errors arising from the lateral inhomogeneity of the wafers, the same samples were used for the optical and XRD investigations.

The photoluminescence (PL) measurements were carried out between $4.2 \leq T \leq 296$ K, using a variable-temperature cryostat. The 514.5-nm line of an Ar^+-ion laser was used as the excitation source. In the photoluminescence excitation (PLE) experiments the MQW was excited with a tunable dye laser using pyridin dye that was pumped by an argon-ion laser. A double-grating monochromator and a cooled, GaAs cathode photomultiplier were used in conjunction with photon counting techniques to disperse and detect the luminescence.

A double crystal diffractometer was used for the XRD investigations. The Cu $K\alpha_1$ radiation was generated by a rotating anode arrangement running at 45 kV and 600 mA and the Cu $K\alpha_2$ radiation was blocked by slits of 0.2 mm in front of and behind the symmetrical (220) channel-cut Ge monochromator. In addition, a 0.2×2-mm^2 slit was placed in front of the sample so that the irradiated area was limited to a size smaller than the sample itself. The diffracted beam was recorded using a NaI:Tl scintillation detector. The smallest step height of the sample (Θ) and detector circle (2Θ) were 0.000 25° and 0.0005°, respectively. The dispersion of the spectrometer agrees with the smallest step height of the detector circle.

III. RESULTS

A. X-ray diffraction

Figure 1 illustrates the rocking curves near the (002) reflection of the GaAs substrate. Satellites are discernible

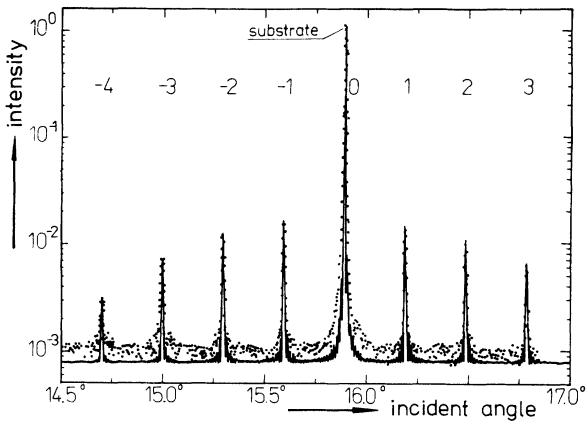

FIG. 1. Diffraction pattern near the (200) reflection of the GaAs substrate recorded on sample 1. The experimental data (points) are compared with the dynamic simulation (curve). Intensity is in abstract units.

from the "−" fourth up to the "+" third order. The strength of the higher-order satellites is below the detection limit due to suppression by the internal thickness ratio of the barrier and well.[10]

Using the angular spacing between two neighboring satellites the period length D_{ML} of a multilayer structure can be calculated (kinematical approximation; symmetrical case):[11]

$$D_{ML} = L_W + L_B = (\sin\Theta / \sin 2\Theta)(n\lambda/\omega_s) , \quad (1)$$

where Θ is the Bragg angle, λ the x-ray wavelength, and ω_s the angular distance to the main peak. The period length of sample 1 amounts to $D_{ML} = 15.7 \pm 0.1$ nm (cf. Fig. 1). The satellite positions and their strength variation versus the order were used in a dynamical simulation program[10] to obtain the MQW parameters, particularly to distinguish L_W and L_B.

The theoretical simulation describes the experimental features using the parameters $L_W = (2.7 \pm 0.2)$ nm and $L_B = (13 \pm 0.2)$ nm for sample 1 (cf. Fig. 1). The barrier composition $x = 0.32$, determined by PL investigations, was employed. Similar results were observed for the other samples. Except for sample 13, the uncertainty of L_W was found to be less than one monolayer. Because of the low Al content ($x = 0.12$) in the XRD pattern of sample 10, only two satellites were resolved. Consequently, we used here the wedge transmission electron-microscopy results [$L_W = (11.6 \pm 0.6)$ nm], which agree well with the XRD findings on other samples.

B. Exciton binding energies

The PL (dotted line) and the PLE (solid line) spectra of sample 8 taken at the same position on the sample at $T = 5$ K are displayed in Fig. 2(a). The PLE spectrum was recorded with the spectrometer positioned on the low-energy side of the main luminescence band [$h\nu_c(\text{det}) = 1.554$ eV); cf. arrow in Fig. 2(a)]. The peaks

in the excitation spectra, which correspond to the excitonic absorption, are labeled with their probable origin. Throughout this paper, the notations *n-mh* and *n-ml* denote excitons with the character of the *n*th electron and *m*th heavy- or light-hole subbands, respectively.

The two most prominent peaks in the PLE spectrum of Fig. 2(a) are evidently the ground-state free excitons associated with the lowest electron and heavy-hole

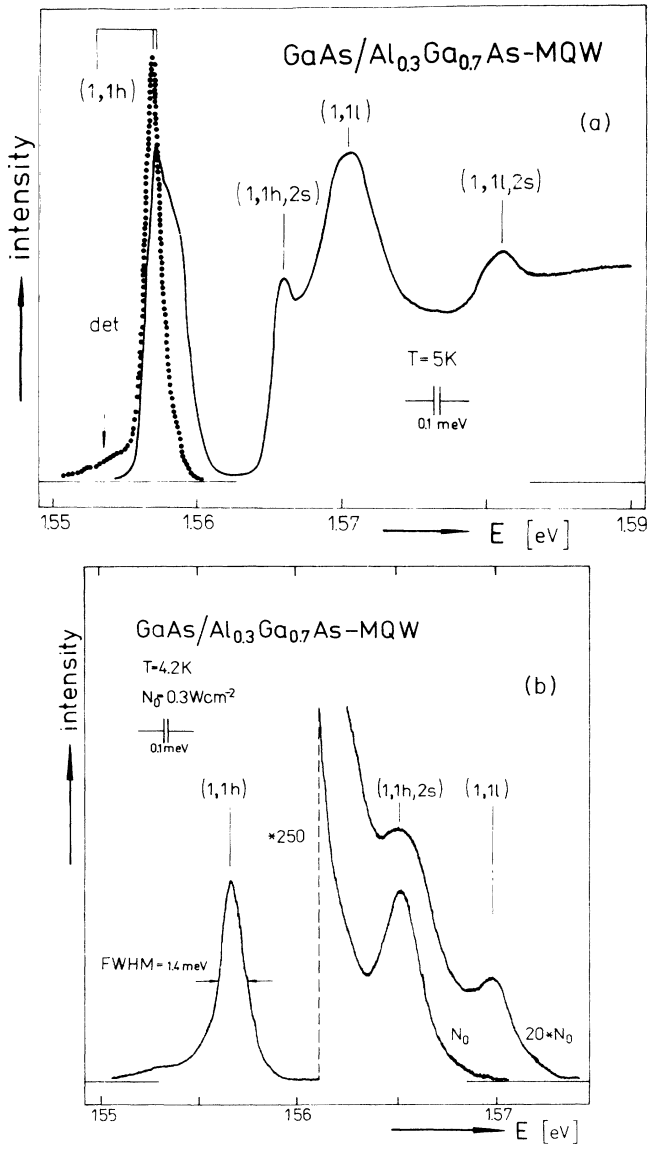

FIG. 2. (a) PL (dotted line) and PLE spectra (solid line) of sample 8 ($L_W=8.8$ nm, $x=0.32$) at $T=5$ K. Along with the heavy-hole $(1,1h)$ and light-hole $(1,1l)$ free excitons the corresponding excited states $(1,1h,2s)$ and $(1,1l,2s)$ are clearly resolved in the PLE spectrum. The Stokes shift is less than 0.5 meV. $h\nu_c(\text{det})=1.554$ eV spectrometer position during PLE measurement. (b) PL spectrum of sample 8 at $T=4.2$ K. The ground state $(1,1h)$ FWHM=1.4 meV and the excited state $(1,1h,2s)$ (250 times higher amplifier sensitivity) of the heavy-hole exciton are clearly resolved at $N_0=0.3$ W cm^{-2}. The ground-state light-hole exciton is discernible with twenty times higher excitation density.

$[h\nu_c(1,1h)=1.5571$ eV] and with the lowest electron and light-hole $[h\nu_c(1,1l)=1.5705$ eV] sublevels.[12-15] Clearly resolved on the high-energy side of each of these excitons are the excited $2s$ states of the heavy-hole $[h\nu_c(1,1h,2s)=1.5659$ eV] and light-hole $[h\nu_c(1,1l,2s)=1.581$ eV] excitons.[12-15] The Stokes shift smaller than 0.5 meV and the observation of four well-defined features in the PLE spectrum attest to the high quality of the sample. However, a very narrow heavy-hole PL band appears whereas the heavy-hole excitation line is broader and with a somewhat irregular shape on the high-energy side, which might be caused by an unresolved fine structure.

PL spectra of the same sample at liquid-helium temperatures are displayed in Fig. 2(b) with the proposed identification of each transition being listed. The dominant feature is the narrow luminescence band $h\nu_c(1,1h)=1.5567$ eV [full width at half maximum (FWHM) =1.4 meV] observed at excitation density ($N_0=0.3$ W cm^{-2}) and $T=4.2$ K. This band was assigned to the ground-state free exciton associated with the lowest electron and hole subbands in the quantum well.

On the high-energy side of the $(1,1h)$ line a band can be resolved (recorded with 250 times higher amplifier sensitivity), which was attributed to the excited state of the heavy-hole free exciton $h\nu_c(1,1h,2s)=1.5654$ eV. Due to the occupation of higher-energy levels with rising excitation density ($N=6$ W cm^{-2}), a band appears on the high-energy side of the spectrum, which is caused by the radiative decay of free excitons connected with the lowest electron and light-hole sublevels $h\nu_c(1,1l)=1.5698$ eV. The assignment of the main low-temperature emission lines as $(1,1h)$, $(1,1h,2s)$, and $(1,1l)$ recombinations has been confirmed by comparing its peak energies with the corresponding exciton peaks in the excitation spectrum.

Figure 3 shows typical PL spectra of sample 4 measured at different temperatures in the range $5 \leq T \leq 125$ K. The spectra have been aligned subtracting the temperature dependent gap of three-dimensional (3D) GaAs $[h\nu_c - E_g^{\Gamma}$ (GaAs); E_g^{Γ}(GaAs) denotes the 3D GaAs gap at different temperatures].[16,17]

The 5-K PL spectrum is caused by the radiative decay of ground-state heavy-hole excitons $[h\nu_c(1,1h)=1.6081$ eV, FWHM=4 meV] associated with the lowest sublevels. In addition to the $(1,1h)$ transition the excited state of the heavy-hole $(1,1h,2s)$ and the ground state of the light-hole $(1,1l)$ exciton are resolved at $T=30$ K. Moreover, the excited-state exciton transition $(1,1l,2s)$ of the light hole was discernible at $T=75$ K. The ground-state light-hole exciton transition intensity continuously increases with rising temperature with respect to the ground-state heavy-hole exciton one, due to the thermal population of the higher sublevels (cf. Fig. 3).

Additional evidence in support of the $2s$ excited-state assignment is provided by the temperature dependence of these peaks. The binding energy of the $2s$ exciton states is $E_b^{hh}(2s)=1.9$ meV and $E_b^{lh}(2s)=2.8$ meV for the heavy and light holes of sample 4, respectively (cf. Ref. 6). As a result, with rising temperatures the $2s$ excitons

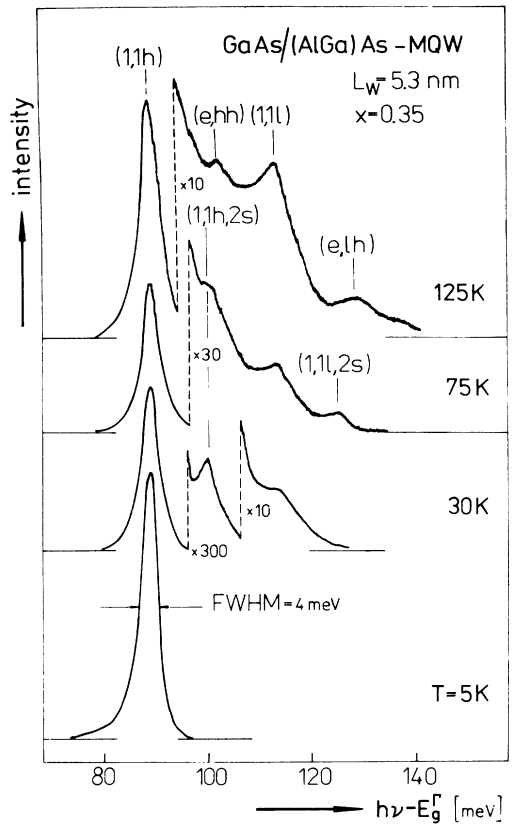

FIG. 3. PL spectra of sample 4 ($L_W=5.3$ nm, $x=0.35$) in the temperature range between $5 \leq T \leq 125$ K and excitation density of $N_0=0.5$ W cm^{-2}. The horizontal axis represents the photon energy minus the energy gap of 3D GaAs (E_g^Γ). The heavy-hole ground-state $(1,1h)$ and excited exciton transition $(1,1h,2s)$ along with the ground-state $(1,1l)$ and excited state $(1,1l,2s)$ light-hole one are resolved. At the highest temperature the free electron-hole sublevel transitions associated with the lowest heavy- (e,hh) and light-hole $(e,\text{1h})$ sublevels are discernible.

are thermally ionized whereas the $1s$ excitons should still be present. At 125 K the free-electron–hole transitions associated with the lowest electron, heavy- (e,hh), and light-hole $(e,\text{1h})$ sublevels are well resolved. The heavy- and light-hole binding energies $E_b(1s)$ can be determined directly as the energy distance between these features and the corresponding ground-state exciton peak positions.

A line-shape analysis would be needed to precisely determine the peak energies of excited states and free-electron–hole sublevel transitions. We observed these transitions in a wide temperature range and the $h\nu_c - E_g^\Gamma$(GaAs) values of the $(1,1h,2s)$, $(1,1l,2s)$, (e,hh), and (e,lh) transitions remain unaltered versus the temperature. Therefore, we use the peak positions as an approximation of the corresponding energy value. However, due to line broadening with increasing temperature the experimental uncertainty increases for the sublevel energy distances determined at temperatures above 100 K.

The experimentally observed results are compared with the predictions of the exciton theory for GaAs/(Al,Ga)As quantum wells[6] in Table I. The calculations of Ref. 6 assume the old Dingle formula $\Delta E_g=1.247x$ (in eV) for the band-gap difference between $Al_xGa_{1-x}As$ and GaAs,[18] and a conduction- to valence-band discontinuity ratio of 65%:35%.

Recently, more accurate results for the band-gap difference have been established.[19–22] However, the sensitivity of the exciton binding energies to a small change of the barrier gap is not greater than a few tenths of a meV. The main dependence of the binding energy on the Al concentrations does not come from the barrier height (except for very narrow wells), but rather from nonparabolicity of the bulk conduction band and the dielectric mismatch between well and barrier materials.[6]

Using the above parameters, the theoretical results of the ground-state heavy- and light-hole exciton binding energies can be fitted by the relation

$$E_b^{\text{hh,lh}}(L_W,x)=\sum_{k=0}^{2}\sum_{j=1}^{4} A_{jk}\frac{x^k}{(L_W+L_0)^j} . \tag{2}$$

This formula describes the theoretical predictions of Ref. 6 with an average accuracy of 0.1 meV in the range $30 \leq L_W \leq 200$ Å; $0.25 \leq x \leq 1$ and with errors up to 0.3 meV in the worst case ($L_W=30$ Å; $x=0.7$). We note that the deviation between relation (2) and the theoretical predictions [cf. full calculations in Ref. 6] is of the order of or smaller than the accuracy of the theory. The coefficients A_{jk} are given in Table II for energies and well widths in units of meV and 10 nm, respectively. The parameter in relation (2) amounts to $L_0=0.5$.

The binding energies $E_b(2s)$ of the excited heavy- and light-hole exciton states are given in Ref. 6 and the corresponding ground-state binding energies can be calculated with the help of (2). Thus the theoretical separations of the $2s$ excited from the $1s$ ground states are obtained by subtracting $E_b(1s)-E_b(2s)$ (cf. columns 5 and 6 in Table I). The deviations between the experimentally and theoretically obtained $1s$-$2s$ energy differences are generally smaller than 1 meV (cf. Table I) and demonstrate both the accurate calculations and measurements. The experimentally observed differences $E_b(1s)-E_b(2s)$ for the heavy-hole (triangles) and light-hole (circles) excitons are compared with the theoretically predicted values (curves for $x=0.32$) in Fig. 4. In addition, values for $x=0.51$ and 1 are shown. We note that the effect of the barrier composition change in the range $0.29 \leq x \leq 0.35$ is within the experimental uncertainty of the given results (in the worst case $L_W=3$ nm about 1 meV for the light-hole excitons).

The $1s$ ground-state exciton binding energies were experimentally determined directly as the energy distance between the electron-hole sublevel and the ground-state exciton transition (cf. columns 7 and 8 in Table I). Figure 5 compares the experimentally observed ground-state exciton binding energies $E_b(1s)$ for the heavy holes (closed triangles) and light holes (closed circles) with the corresponding theoretical predictions (curves calculated for $x=0.29$ and 0.32). Values for $x=0.51$ and 1 are additionally displayed. In the case where only the $2s$ excited-state transition was resolved we add the small and weakly L_W-dependent binding energy $E_b(2s)$ [$1.6 \leq E_b^{\text{hh}}(2s) \leq 2.1$

TABLE I. L_W well width in nm, x AlAs mole fraction of the barriers. Energy distance between the $2s$ and $1s$ states $[E_b(1s)-E_b(2s)]$ and ground-state exciton binding energy $E_b(1s)$ (in meV) of heavy-hole $(1,1h)$ and light-hole $(1,1l)$ free excitons.

No.	L_W (nm)	x		$E_b(1s)-E_b(2s)$ (meV) $(1,1h)$	$(1,1l)$	$E_b(1s)$ (meV) $(1,1h)$	$(1,1l)$
1	2.7	0.32	exp.	11.7		14.5	
			calc.	11.7	14.4	14.0	16.5
2	3.5	0.29	exp.	11.1	13.5	13.2	
			calc.	11.0	12.9	13.1	15.5
3	4.5	0.32	exp.	10.5		12.6	
			calc.	10.6	12.8	12.5	15.5
4	5.3	0.35	exp.	10.3	12.2	12.5	15.0
			calc.	10.2	12.5	12.3	15.3
5	6.5	0.32	exp.	9.7	11.3	11.2	14.1
			calc.	9.5	11.5	11.2	14.1
6	7.6	0.29	exp.	9.0	10.5		13.1
			calc.	8.7	10.6	10.5	13.1
7	7.9	0.35	exp.	9.2			
			calc.	8.8	10.7	10.7	13.5
8	8.8	0.32	exp.	8.5	10.2		
			calc.	8.4	10.1	10.2	12.7
9	11.9	0.35	exp.	7.4			
			calc.	7.5	8.7	9.2	11.3

meV in the range $12 \geq L_W \geq 3$ nm] to the experimentally observed value to get the continuum edge energy (open circles in Fig. 5).

The agreement between the experimental and theoretical findings is excellent for both the heavy- and light-hole excitons and in the whole well width range investigated. It is worth noting that there is no parameter to align the theoretical prediction to the experimental data. Considering this agreement we expect a reliable $1s$ ground-state binding energy predicted by the theory given in Ref. 6 or by relation (2).

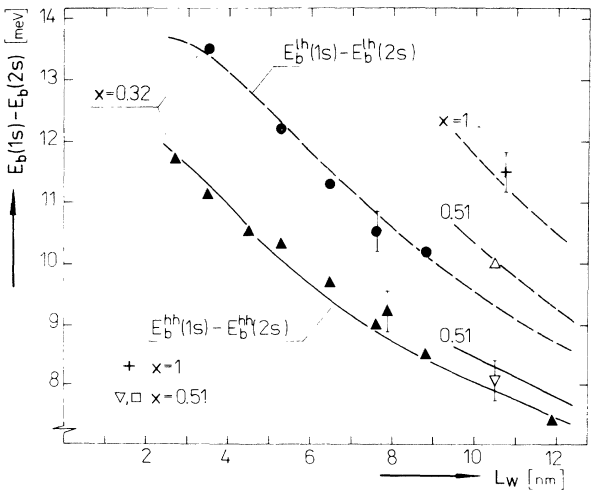

FIG. 4. Energy distance between the ground- and excited-state heavy-hole (triangles; solid lines) and light-hole (circles; dashed lines) excitons associated with the lowest sublevels versus the well thickness. The theoretical results (curves) were calculated for $x=0.32$ using Eq. (2). Results for $x=0.51$ and 1 are additionally shown.

C. Transition energies

PL and PLE spectra of sample 11 are shown in Fig. 6(a). The peak labels are chosen to refer to the originating recombination process. The PL spectrum shows a split exciton feature caused by monolayer fluctuations at the interface. From the PLE we obtain that the thinner parts of the well dominate. The two most prominent peaks in the PLE spectrum are evidently the ground-state free excitons associated with the $n=1$ electron and heavy-hole $[h\nu_c(1,1h)=1.5420$ eV (FWHM$=1.4$ meV)] and with the light-hole $[h\nu_c(1,1l)=1.5515$ eV] sublevels.

The well-resolved (FWHM$=4$ meV) excitons at $h\nu_c(2,1l)=1.6260$ eV and $h\nu_c(2,2h)=1.6324$ eV are associated with the second $(n=2)$ electron and first light-hole as well as the second heavy-hole sublevel. The "forbidden" $(2,1l)$ transition, which can only be observed in a $2p$ state, has 1.5 times higher strength than the $(2,2h)$ one that agrees with oscillator strength calculations involving

TABLE II. Coefficients A_{jk} for interpolation formula (1) of heavy- and light-hole ground-state exciton binding energies calculated in Ref. 6. The energies are given in meV if the well widths are taken in units of 10 nm. The parameter L_0 amounts to 0.5.

Exciton	j	$k=0$	$k=1$	$k=2$
$(1,1h;1s)$	1	27.909	3.325	−1.163
	2	−38.131	3.552	3.593
	3	30.417	−5.075	−5.232
	4	−10.389	6.289	0.789
$(1,1l;1s)$	1	31.401	−5.739	0.091
	2	−40.120	41.440	1.656
	3	27.250	−19.564	−29.228
	4	−8.960	3.849	19.393

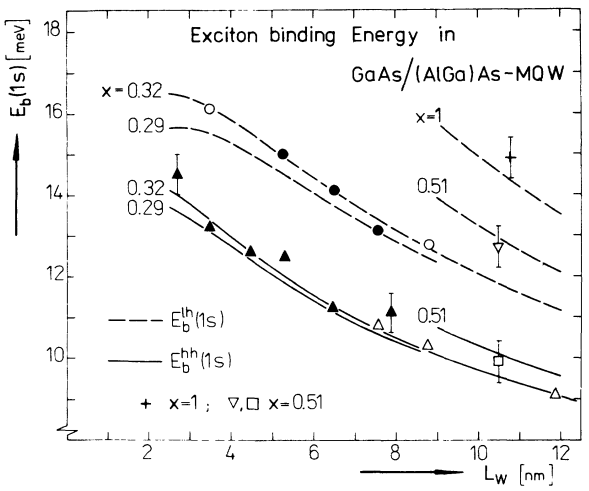

FIG. 5. Ground-state binding energies of the light-hole $[E_b^{lh}(1s)]$ and heavy-hole $[E_b^{hh}(1s)]$ excitons associated with the lowest sublevels versus the well width L_W; experimental data (closed circles) and theoretical predictions (curves). Theoretical curves are given for $x=0.32$ and 0.29 for the heavy-hole (solid lines) and light-hole (dashed lines) excitons. Results for $x=0.51$ and 1 are additionally shown. In some cases (cf. text) $E_b(2s)$ was added to $h\nu_c(1,1l,h,2s)$ to get $E_b(1s)$ (open data points).

the valence-band mixing via the calculated valence-band structure and via Coulomb coupling between excitons belonging to different sublevels.[23] Figure 6(b) displays PL spectra of the same sample. Owing to the thermalization of the carriers with increasing temperature all expected transitions associated with the confined first and second electron levels can be resolved. It is worth noting that the reduced peak energies $[h\nu_c - E_g^{\Gamma}(\mathrm{GaAs})]$ observed by PL and PLE agree excellently with each other.

Figure 7 shows the PL spectra of sample 5 at different temperatures between 60–296 K. Note the intensity covers over six orders of magnitude for each spectrum. The most prominent peaks at $h\nu_c(1,1h) - E_g^{\Gamma}(\mathrm{GaAs}) = 65.5$ meV and $h\nu_c(1,1l) - E_g^{\Gamma}(\mathrm{GaAs}) = 85.9$ meV are due to the recombination of free heavy- and light-hole excitons associated with the lowest sublevels. Four additional peaks are assigned to the $(1,3h)$, $(2,1l)$, $(2,2h)$, and $(2,2l)$ free exciton transitions due to recombinations in the well. This completes all the expected ground-state excitonic recombinations associated with the sublevels confined in this well. The luminescence band (X) at peak energy $h\nu_c(X) = 1.974$ eV ($T=60$ K) is caused by the radiative decay of excitons in the barrier and corresponds to an Al content of $x=0.32$ [cf. Ref. 9]. At increased temperature the exponential tail, mainly due to the free-electron–hole recombination, becomes more pronounced and begins to submerge the higher-energy peaks. At room temperature the high-energy tail dominates the high-energy spectral range. However, the ground-state free exciton recombinations $(1,1h)$ and $(1,1l)$ are still prominent, by a factor of 5 or more intense than the sublevel free carrier recombination.

V. DISCUSSION AND CONCLUSIONS

In examining Table III, which compares the measured and calculated excitonic peak energy shifts $h\nu_c - E_g^{\Gamma}(\mathrm{GaAs})$ due to the exciton confinement, the conclusions are the following: Figure 8 presents the energy separation between the light- and heavy-hole ground-state exciton transitions $[\delta E = h\nu_c(1,1l) - h\nu_c(1,1h)]$ versus well width. The energy separation between the

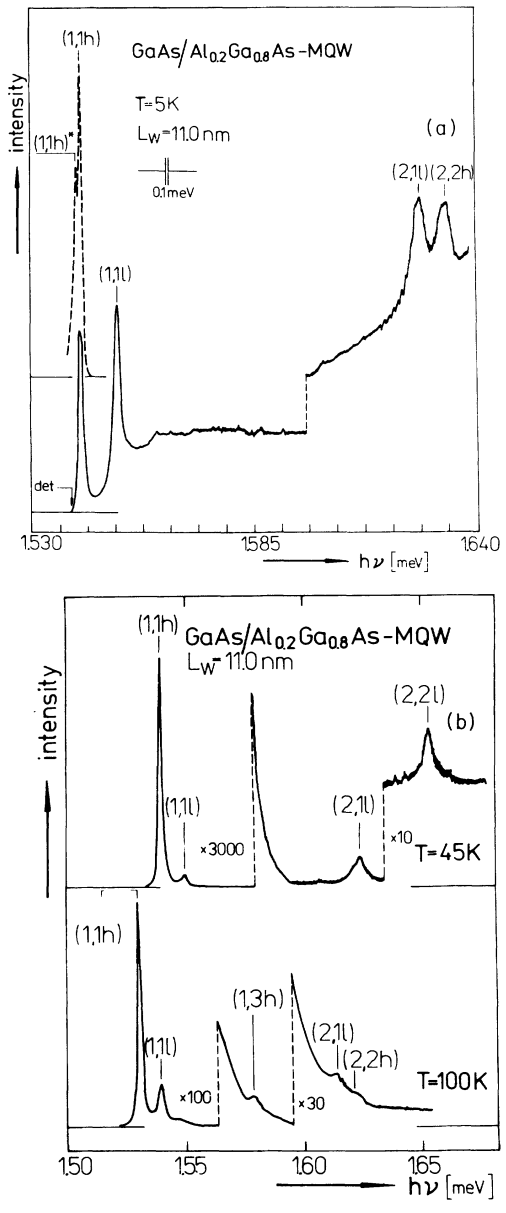

FIG. 6. (a) PL (dashed line) and PLE (solid line) spectra of sample 11 ($L_W=11.0$ nm, $x=0.20$) at $T=5$ K. The split exciton in the PL $[(1,1h)^*$ and $(1,1h)]$ is due to monolayer fluctuations at the interface. This assignment was confirmed by measurements with increasing temperature, which indicates the exciton transfers from thicker into thinner well regions. (b) PL spectra of sample 11 at $T=45$ and 100 K, excitation density 0.3 W cm^{-2}. The numbers represent the amplification step height.

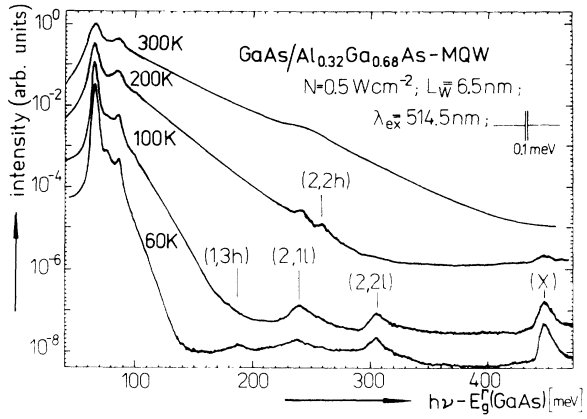

FIG. 7. PL spectra of sample 5 ($L_W=6.5$ nm, $x=0.32$) at different temperatures in semilogarithmic scale. The horizontal axis represents the photon energy minus the energy gap of 3D GaAs (E_g^Γ).

light- and heavy-hole sublevels depends on the valence-band offset. Consequently, the value δE is sensitive to changes in the ratio $\Delta E_C:\Delta E_V$. Near $k=0$ the split-off valence band repels the light-hole band only and δE decreases. To illustrate these features the calculations including the split-off–light-hole valence-band (SOVB) interaction [cf. Ref. 5] and different values ΔE_C are displayed in Fig. 8. In addition, a simulation neglecting the SOVB interaction is shown ($\Delta E_C=0.7\Delta E_g$). The calculations including the SOVB interaction and a conduction-band offset $\Delta E_C=0.7\Delta E_g$ (solid line) excellently agree with the experimental data, whereas one's neglecting SOVB or using $\Delta E_C=0.65\Delta E_g$ predicts δE too large, outside the experimental uncertainty, especially for thin wells (cf. dotted and dashed lines).

This result supports the offset ratio $\Delta E_C:\Delta E_V=0.7:0.3$ that was experimentally determined by optical examination of low confined states under hydrostatic pressure.[24] This deduction depends on the details of the theoretical

TABLE III. L_W well width in nm, x AlAs mole fraction of the barriers. Reduced transition energies $h\nu_c-E_g^\Gamma$ (GaAs) (in meV) of free excitons associated with the lowest electron and heavy-hole $(1,1h)$, lowest electron and light-hole $(1,1l)$, second electron and lowest light-hole $(2,1l)$, second electron and heavy-hole $(2,2h)$, and second electron and light-hole $(2,2l)$ sublevels. The exciton binding energies are given in parentheses.

No.	L_W (nm)	x		$(1,1h)$	$(1,1l)$	$(2,1l)$	$(2,2h)$	$(2,2l)$
10	11.6	0.12	exp.	17.3	24.3	81.1	88.0	
			calc.	17.3	24.2	87.6	93.7	
				(8.4)	(9.9)	(4.7)	(4.1)	
11	11.0	0.20	exp.	22.8	32.3	106.8	113.2	135.8
			calc.	22.4	31.0	107.1	113.2	150.6
				(9.1)	(11.0)	(5.7)	(5.4)	(5.1)
12	10.5	0.51	exp.	31.5	43.6	138.0	145.0	
			calc.	30.2	41.5	138.6	147.4	
				(10.1)	(12.3)	(7.9)	(5.6)	
13	10.7	1	exp.	35.2	49.4	154.2	170.3	
			calc.	31.0	42.5	145.0	156.2	
				(11.2)	(14.3)	(9.7)	(6.5)	
1	2.7	0.32	exp.	191.8	223.8			
			calc.	189.9	222.4			
				(14.0)	(16.5)			
2	3.5	0.29	exp.	138.9	167.3			
			calc.	138.7	167.1			
				(13.0)	(15.5)			
3	4.5	0.32	exp.	105.8	131.8		320.0	
			calc.	108.2	134.4		347.0	
				(12.5)	(15.5)		(5.6)	
5	6.5	0.32	exp.	66.4	86.0	238.5	257.0	304.0
			calc.	64.1	83.0	244.6	262.3	331.5
				(11.2)	(14.1)	(5.9)	(8.2)	(5.0)
6	7.6	0.29	exp.	48.7	64.1	180.2	196.3	
			calc.	48.2	63.6	195.2	209.9	
				(10.5)	(13.1)	(6.1)	(5.6)	
8	8.8	0.32	exp.	38.7	51.9	158.0	166.0	214.0
			calc.	38.9	52.3	166.7	176.2	233.1
				(10.2)	(12.7)	(6.7)	(7.6)	(6.0)

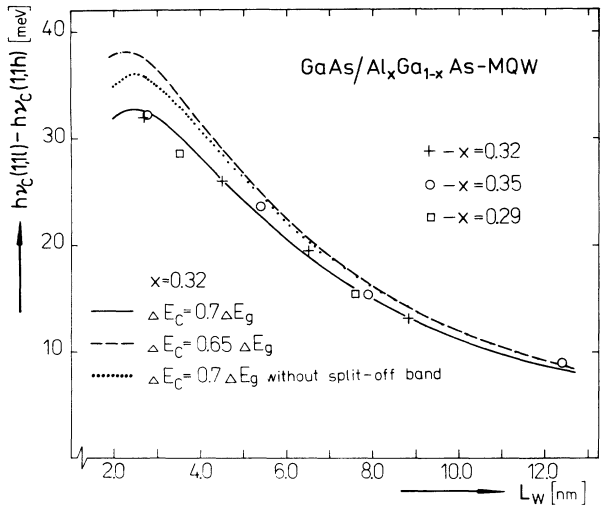

FIG. 8. Energy distance between the $(1,1l)$ and $(1,1h)$ transitions vs the well width. Experimental data are shown for $x=0.29$ (□), 0.32 (+), and 0.35 (○). The curves were calculated for $x=0.32$ including $\Delta E_C=0.7\Delta E_g$ with (solid line) and without (dotted line) split-off–light-hole valence-band (SOVB) interaction. The calculation with SOVB interaction and $\Delta E_C=0.65\Delta E_g$ is additionally shown (broken line).

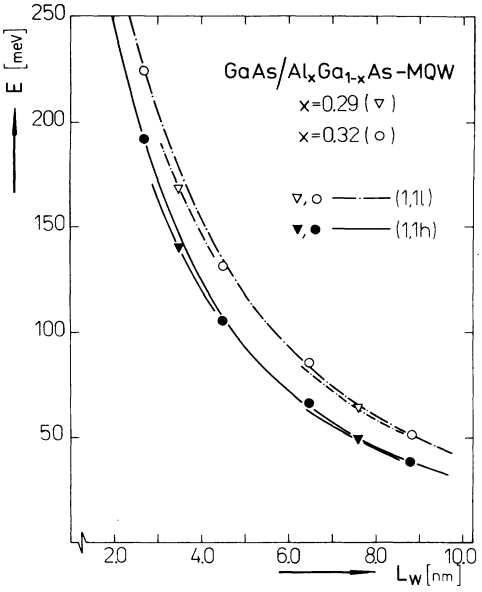

FIG. 9. Heavy- (closed points) and light-hole (open points) exciton transition energies of the samples 1,2,3,5,6,8 [$x=0.29$ (triangles) and $x=0.32$ (circles) cf. Table III] vs the independently observed well width. The curves were calculated for the heavy- (solid line) and light-hole (chain line) transitions using the parameters given in the text and for $x=0.32$ as well as $x=0.29$ (partly).

model chosen. In this work, the influence of the split-off band was calculated in second-order perturbation theory and at the same time a parabolic light-hole band was assumed. Indeed, the conclusion about the offset ratio would not be essentially changed by inclusion of the light-hole nonparabolicity, whose effect was found to be more than three times smaller than that of the coupling to the split-off band.

The peak energies of the transitions $(1,1h)$ and $(1,1l)$ are listed in Fig. 9 versus the independently observed well width. Two things should be noted: (i) the transition energies change by a factor of 5 in the range investigated, and (ii) the 10-monolayer-thick well approaches the validity limit of the effective-mass theory. Nevertheless, the agreement between the experimental and theoretical results is excellent for the heavy- and light-hole exciton transitions in the whole thickness range investigated. This agreement demonstrates the reliability of the experiments and the theoretical approach including the offset value of $\Delta E_C=0.7\Delta E_g$ (Ref. 24) and the SOVB interaction.[5] Using these calculations, the energies of the lowest electron, heavy- and light-hole sublevels with respect to the 3D GaAs gap can be fitted by the relation

$$E_{e,\mathrm{hh,lh}}(L_W,x)=\sum_{k=0}^{3}\sum_{j=1}^{4}A_{jk}\frac{x^k}{(L_W+L_0)^j}\ . \tag{3}$$

This formula describes the theoretically predicted sublevel energies in the range $2.5\le L_W\le 12$ nm; $0.1\le x\le 0.5$ with an average accuracy of 0.1 meV [worst case 0.2 meV for ($x=0.1$; $L_W=3.8$ nm)], 0.15 meV [0.4 meV ($x=0.25$; $L_W=2.6$ nm)], and 0.2 meV [0.5 meV ($x=0.5$; $L_W=12$ nm)] for the heavy holes, light holes, and electrons, respectively. The coefficients A_{jk} and parameters L_0 are given in Table IV.

Considering now the excitons associated with the higher ($n=2$) electron level. Comparing the values within Table III we recognize a systematic trend: Nearly all calculated transition energies involving the second electron $h\nu_c(2,\mathrm{mhl})^{\mathrm{cal}}$ level are greater than the experimentally observed $h\nu_c(2,\mathrm{mhl})^{\mathrm{exp}}$ one $[h\nu_c(2,\mathrm{mhl})^{\mathrm{cal}}-h\nu_c(2,\mathrm{mhl})^{\mathrm{exp}}=\Delta\epsilon>0]$.

TABLE IV. Coefficients A_{jk} for interpolation of the lowest electron (ϵ_{e1}), heavy-hole (ϵ_{hh1}), and light-hole (ϵ_{lh1}) sublevel energies using Eq. (3). The energies are given in meV if the well width is taken in units of 10 nm. The parameters L_0 amount to 0.5325, 0.5035, and 0.7049 for the electron, heavy-hole, and light-hole sublevels, respectively.

Sublevel	j	$k=0$	$k=1$	$k=2$	$k=3$
Electron	1	21.0300	−1.9384	−232.3450	451.0892
ϵ_{e1}	2	−24.7774	180.8804	−289.1602	127.7617
	3	66.7841	203.6167	−334.5747	−166.0166
	4	−42.3846	9.9876	187.0574	28.7673
Heavy-hole	1	4.6838	0.2104	−57.2411	21.2893
ϵ_{hh1}	2	−11.3998	27.3533	144.9361	9.9938
	3	32.1678	−26.9544	−233.0475	13.0987
	4	−16.7558	70.3640	29.5898	23.2258
Light-hole	1	17.7688	−70.0193	64.5475	243.6362
ϵ_{lh1}	2	−22.7024	179.1406	−393.8990	−188.3782
	3	58.8663	257.7219	−244.8422	−46.4185
	4	−48.2929	40.2566	212.6958	123.0737

It is well known that the nonparabolicity of the conduction band included in the bulk dispersion relation and in the boundary condition shifts the $n=2$ electron sublevels much more strongly than the $n=1$ electron sublevels.[25] Considering this behavior it would be tempting to explain the observed deviation by an incorrect description of the conduction-band nonparabolicity. Consequently, we would expect an increasing $\Delta\epsilon$ with a growing second electron level energy. In contrast we observe that (i) for the $(2,1l)$ and $(2,2h)$ transitions $\Delta\epsilon$ decreases with increasing energy of the $n=2$ electron level between different samples (cf. samples 10–12 in Table III), and (ii) although the same electron level is involved in the $(2,1l)$ and $(2,2l)$ excitons, $\Delta\epsilon$ increases with growing energy of the transitions observed on the same sample (cf. samples 2, 8, and 10). Therefore, we rule out an incorrect description of conduction-band nonparabolicity as an explanation of the apparent energetic discrepancies.

In conclusion, the ground-state exciton binding energies were found in excellent agreement between experiment and theory. Using these values the $(1,1h)$ and $(1,1l)$ transition energies excellently agree with the theoretical predictions that include the split-off–light-hole valence-band interaction. Interpolation formulas are given for the calculation of the lowest electron, heavy- and light-hole sublevels as well as for the heavy- and light-hole ground-state exciton binding energies. Deviations between experiment and theory especially for the higher ($n=2$) levels might be connected with a nonsquare potential model based on well imperfections.[26–29] More detailed studies of the interface are obviously needed to answer the questions raised by the presented investigations.

ACKNOWLEDGMENTS

This work was made possible through grants from the Deutsche Forschungsgemeinschaft (No. IIC3-Oe 16112-1). The authors want to thank R. Riedel for her technical assistance.

APPENDIX

The QW energy sublevels are calculated using an envelope-function approach.[30] At $k=0$ the finite barrier solution for the square well is[31]

$$\frac{\sqrt{2m_W^* E}}{m_W^*}\sin\left(\sqrt{m_W^* E/2}\right) - \frac{\sqrt{2m_B^*(V-E)}}{m_B^*}\cos\left(\sqrt{m_B^* E/2}\right)=0 ,$$

where m_W^* and m_B^* are the well and barrier effective masses (in units of m_0), E is the sublevel energy, and V is the barrier potential (band offset). Bulk nonparabolicity is taken into account via energy-dependent electron masses [cf. Ref. 32] $m_e^*=m^*/[1-E/\beta]$ for the well and $m_e^*=m^*/[1-(E-V)/\beta]$ for the barrier [$m^*=0.0665+0.0835x$ (Ref. 33). β by coincidence has the value of the fundamental gap $E_g^{\Gamma}(x)=1.5192+1.42x$ (eV).[19] The hole masses are determined from the Luttinger parameters,[34] $m_{\rm hh}^*=(\gamma_1-2\gamma_2)^{-1}$ and $m_{\rm lh}^*=(\gamma_1+2\gamma_2)^{-1}$ ($\gamma_1=6.85-4.75x$ and $\gamma_2=3.45-2.77x$ (Ref. 32). The split-off [$\Delta E_{\rm so}=0.340-0.05x$ (eV)] light-hole band interaction is included via a second-order perturbation calculation on the Luttinger Hamiltonian.

*Present address: HASYLAB at DESY, Notkestr.85, DW-2000 Hamburg 52, Germany.

[1] Y. Fu and K. A. Kao, Phys. Rev. B **40**, 8349 (1989).

[2] D. S. Chu and Ying-Chih Lou, Phys. Rev. B **43**, 14 504 (1991).

[3] H. Mathieu, P. Lefebvre, and Ph. Christol, Phys. Rev. B **46**, 4092 (1992).

[4] N. H. Ky, J. D. Ganiére, M. Gailhanou, F. Morier-Genoud, D. Martin, and F.-K. Reinhart, Phys. Rev. B **46**, 6947 (1992).

[5] U. Ekenberg, L. C. Andreani, and A. Pasquarello, Phys. Rev. B **46**, 2625 (1992).

[6] L. C. Andreani and A. Pasquarello, Phys. Rev. B **42**, 8928 (1990).

[7] M. Gurioli, J. Martinez-Pastor, M. Golocci, A. Bosacchi, S. Franchi, and L. C. Andreani, Phys. Rev. B **47**, 15 755 (1993).

[8] L. C. Andreani, A. D'Andrea, and R. Del Sole, Phys. Lett. **168**, 451 (1992).

[9] G. Oelgart, G. Lippold, R. Heilmann, H. Neumann, and B. Jacobs, Phys. Status Solidi A **115**, 257 (1989).

[10] T. Baumbach, H. G. Brühl, H. Rhan, and U. Pietsch, J. Appl. Crystallogr. **21**, 386 (1988).

[11] V. S. Sperioso, M. A. Nicolet, J. C. Tandon, and Y. C. M. Yeh, J. Appl. Phys. **57**, 1377 (1985).

[12] P. Dawson, K. J. Moore, G. Duggan, H. I. Ralph, and C. T. B. Foxon, Phys. Rev. B **34**, 6007 (1986).

[13] E. S. Koteles and J. Y. Chi, Phys. Rev. B **37**, 6332 (1988).

[14] F. Laruelle and B. Etienne, Solid State Commun. **65**, 565 (1988).

[15] L. W. Molenkamp, G. W. E. Bauer, R. Eppenga, and C. T. Foxon, Phys. Rev. B **37**, 6332 (1988).

[16] E. Grilli, M. Guzzi, R. Zamboni, and L. Pavesi, Phys. Rev. B **45**, 1638 (1992).

[17] G. Oelgart, B. Orschel, M. Proctor, D. Martin, F. Morier-Genoud, and F.-K. Reinhart, J. Appl. Phys. **74**, 2742 (1993).

[18] R. Dingle, R. A. Logan, and J. R. Arthur, Jr., *Gallium Arsenide and Related Compounds,* IOP Conf. Proc. No. 33A (Institute of Physics and Physical Society, London, 1976), p. 210.

[19] G. Oelgart, R. Schwabe, M. Heider, and B. Jacobs, Semicond. Sci. Technol. **2**, 468 (1987).

[20] T. F. Kuech, D. J. Wolford, R. Potemski, J. A. Bradley, K. H. Kelleher, D. Yan, J. P. Farrell, P. M. S. Lesser, and F. H. Pollak, Appl. Phys. Lett. **51**, 505 (1987).

[21] B. Lambert, J. Caulet, A. Regreny, M. Baudet, B. Deveaud, and A. Chomette, Semicond. Sci. Technol. **2**, 491 (1987).

[22] C. Bosio, J. L. Staehli, M. Guzzi, G. Burri, and R. A. Logan, Phys. Rev. B **38**, 3263 (1988).

[23] L. C. Andreani and A. Pasquarello, Superlatt. Microstruct. **5**, 59 (1989).

[24] D. J. Wolford, T. F. Kuech, J. A. Bradley, M. A. Gell, D. Ninno, and M. Jaros, J. Vac. Sci. Technol. B **4**, 1043 (1986).

[25] L. C. Andreani and A. Pasquarello, in *Highlights on Spectros-*

copies of Semiconductors and Insulators, edited by A. Balazarotti, G. Guizetti, and A. Stella (World Scientific, Singapore, 1987), p. 33.
[26]B. Jusser and F. Mollot, Appl. Phys. Lett. **61**, 423 (1992).
[27]D. F. Nelson, R. C. Miller, C. W. Tu, and S. K. Sputz, Phys. Rev. B **36**, 8063 (1987).
[28]R. Sauer, S. Nilsson, P. Roentgen, W. Heuberger, V. Graf, R. Hangleitner, and R. Spycher, Phys. Rev. B **46**, 9525 (1992).
[29]N. G. Asmar and E. G. Gwinn, Phys. Rev. B **46**, 4752 (1992).
[30]M. Alterelli, in *Envelope Function Approach to Electronic States in Interfaces, Quantum Wells, and Superlattices,* edited by C. R. Leaven and R. Taylor (Plenum, New York, 1988).
[31]L. C. Andreani, A. Pasquarello, and F. Bassani, Phys. Rev. B **36**, 5887 (1987).
[32]U. Rössler, Solid State Commun. **65**, 1279 (1988).
[33]M. Guzzi and J. L. Staehli, in *Physics of DX Centers in III-V Ternary Compounds,* edited by J. C. Bourgoin (TransTech, Aedermannsdorf, 1989).
[34]J. M. Luttinger and W. Kohn, Phys. Rev. **97**, 869 (1955).